Design and fabrication of a microplatform for the proximity effect study of localized ELF-EMF on the growth of *in vitro* HeLa and PC-12 cells

2010 J. Micromech. Microeng. 20 125023

(http://iopscience.iop.org/0960-1317/20/12/125023)

J. Micromech. Microeng. **20** (2010) 125023 (10pp) doi:10.1088/0960-1317/20/12/125023

Design and fabrication of a microplatform for the proximity effect study of localized ELF-EMF on the growth of *in vitro* HeLa and PC-12 cells

Y C Chen[1], C C Chen[1], W Tu[2], Y T Cheng[1] and F G Tseng[2]

[1] Department of Electronics Engineering & Institute of Electronics, National Chiao Tung University, Hsinchu 300, Taiwan
[2] Department of Engineering and System Science, National Tsing Hua University, Hsinchu 300, Taiwan

E-mail: ytcheng@mail.nctu.edu.tw

Received 21 September 2010
Published 22 November 2010
Online at stacks.iop.org/JMM/20/125023

Abstract

This paper presents a platform technology with experimental results that show the scientists and biologists a way to rapidly investigate and analyze the biological effects of localized extremely low frequency (ELF) electromagnetic field (EMF) on living cells. The proximity effect of the localized ELF-EMF on living cells is revealed using the bio-compatible microplatform on which an on-glass inductive coil array, the source of the localized ELF-EMF in micro scale, is designed, fabricated and operated with a field strength of 1.2 ± 0.1 mT at 60 Hz for cell culturing study. After a 72 h ELF-EMF exposure, HeLa (human cervical cancer) and PC-12 (rat pheochromocytoma) cells exhibit about 18.4% and 12.9% cell proliferation rate reduction, respectively. Furthermore, according to the presented dynamic model, the reduction of the proliferation can be attributed to the interference of signal transduction processes due to the tangential currents induced around the cells.

(Some figures in this article are in colour only in the electronic version)

1. Introduction

Biological effects on living cells and tissues caused by extremely low frequency (ELF) electromagnetic field (EMF) exposure have gathered research attention in recent years due to the extensive usage of portable personal electronic appliances in our daily life. So far, several studies have shown that the field exposure could result in the change of cell proliferation rate and the incidence of cancer cells [1–4]. For instance, Khalil *et al* found significant suppression of mitotic activity and high incidence of chromosomal aberrations of human lymphocytes under a pulsed 50 Hz, 1.05 mT EMF exposure [5]. Kwee *et al* observed an increase in the proliferation rate of human epithelial amnion cells exposed to a sinusoidal 50 Hz, 80 μT EMF [6]. Wolf *et al* reported that there is about 20–30% increase in proliferation of human promyelocytic leukemia HL-60 cells with a sinusoidal 50 Hz, 1 mT magnetic field (MF) exposure [7]. The exposure can also result in DNA damage of normal WI-38 human embryonic lung fibroblasts. On the other hand, Hoffmann *et al* reported a significant reduction of the cell proliferation rate in dentate granule cells cultured in a 50 Hz EMF field. Buemi *et al* found a gradual decrease in the apoptosis and proliferation rate of renal cells exposed to a 0.5 mT static MF [8]. Huang *et al* proposed that the ELF-MF with field strength below a few mT could significantly inhibit cell growth due to a large attenuation coefficient for ion's movement [9]. Meanwhile, *in vivo* bio-chips have recently become a potential and critical diagnostic instrument which could function with wireless data transmission and power transfer for long-term body health-monitoring applications [10–12]. Since the biological effects affected by the time-variant EMF would be dramatically different due to cell types, field characteristics and possible proximity effects on *in vivo* chips, it is imperative to investigate the correlation and influence of the 'localized' EMF on living cells of the human body.

A lab-on-a-chip scheme has been extensively utilized in the field of biotechnology with several advantages, such as shorter analyzing time, less sample consumption and lower manufacture cost, because scientists could achieve the demands of integration of multiple steps with complicated analytical procedures in a tiny working area for micro-scaled analysis [13, 14]. A miniaturized platform in the scheme can also provide better culturing control to imitate an *in vivo* growth environment in terms of small shear stress, and can simultaneously modify the environment for different cells within a single chip for comparative investigation [15–17]. Thus, in order to investigate the proximity effect of the localized ELF-EMF on living cells and understand related biological effects, a microplatform with on-glass spiral inductors will be presented in the paper to generate localized fields at specified locations for cell culturing study. A concentrated ELF-EMF is generated at the central area of an inductor where the cells can be cultured under conditions mimicking the operational environment of *in vivo* bio-chips. Since the field strength is modified by varying input current and the cell culturing environment could be precisely controlled in the platform, it is our belief that the platform technology and experimental results can help scientists rapidly investigate and analyze the biological effects of the ELF-EMF on living cells. In this paper, HeLa and PC-12 cells are adopted for the preliminary ELF-EMF effect study since both HeLa and PC-12 cells have been representative cells for ELF-EMF investigations [18, 19].

2. Theory of biological effects by ELF-EMF exposure

It has been well known that a large number of free ions, such as K^+, Na^+, Ca^{2+} and Cl^-, exist in the vicinity of both extracellular and intracellular regions of a cell's plasma membrane, so there will be a concentration gradient and voltage difference between two sides of the membrane to control cell functions via signal transduction processes. In an equilibrium state, the net ion flux through the membrane should be zero and the voltage difference built in between the membrane would also reach a critical value of −12 mV in HeLa cells [20] or −60 mV in PC-12 cells [21] where the intracellular voltage is a negative value relative to the extracellular one. In the signal transduction process, cationic electrosensitive channel-proteins play an important role in the generation of the potential gradients [22]. The electrostatic interaction between the voltage sensor in a voltage-gated channel and the transmembrane caused by the concentration difference of cations between the internal and external membrane will determine the switching voltage of the voltage-gated channel [23]. Therefore, by applying a time-variant EMF for changing the electrochemical balance of the plasma membrane, the signal transduction process should be perturbed possibly with the induction of biophysical effects. From Maxwell's equations, a time-variant MF formed in a space would be concurrent with an induced time-variant electric field (EF) and vice versa. The concurrence of both fields is physically called a time-variant EMF. In order to well understand the proximity effect of an ELF-EMF on living cells, the time-variant MF and induced EF associated with the ELF-EMF are then separately employed for the analysis.

2.1. Time-variant MF effect

By considering the Lorentz force acting on the free ions in the vicinity of a plasma membrane, the restoring force, the damping force and the equation of ion motion in a time-variant MF can be depicted as follows [9, 23]:

$$m\ddot{\vec{r}} + \lambda\dot{\vec{r}} - zq\dot{\vec{r}} \times \vec{B} + D\vec{r} = 0, \tag{1}$$

where m, r, λ, z, q and D are the mass and displacement of the free ions, the attenuation coefficient for ionic motion, the valence of ion, the charge element and the restoring constant, respectively. The time-variant MF, $\vec{B}$, has the value of $B_0 \cos \omega t$ where B_0 and ω are the amplitude and angular frequency, respectively, describing the oscillating behavior of this field. For typical ions, like sodium ions in the channel, the mass, attenuation coefficient and self-resonant frequency are of the order of 10^{-26} kg, 10^{-12} kg s^{-1} and 10^{-1} Hz [9], respectively. Since the attenuation coefficient with an order of 10^{-26} is much larger than the restoring constant which is $m\omega^2$, the restoring term in (1) can be safely eliminated. With the initial conditions $r|_{t=0} = 0$ and $\dot{r}|_{t=0} = v_{\text{th}}$, where v_{th} is average thermal velocity, the oscillating displacements can be derived as follows [9]:

$$x_B = \frac{\sqrt{3mkT}}{\lambda - zqB_0 \cos \omega t}\left(1 + e^{-\frac{\lambda - zqB_0 \cos \omega t}{m}t}\right), \tag{2}$$

$$y_B = \frac{\sqrt{3mkT}}{\lambda + zqB_0 \cos \omega t}\left(1 + e^{-\frac{\lambda + zqB_0 \cos \omega t}{m}t}\right), \tag{3}$$

$$z_B = \frac{\sqrt{3mkT}}{\lambda}\left(1 + e^{-\frac{\lambda}{m}t}\right), \tag{4}$$

where k and T are Boltzmann's constant and the environment temperature, respectively.

It should be emphasized that equations (2) and (3) represent the normal and tangential oscillating displacements related to the surface of the plasma membrane. Equation (4) represents temperature-dependent displacement regardless of the applied MF. For instance, the temperature-dependent displacement of the Na^+ ion in the vicinity of the extracellular membrane has a value of 4.4×10^{-11} m for a tangential movement at 37 °C. The estimated mean free path of ions according to equation (4) has the value of the order of 10^{-10} m, which is very close to the proposed values of ions in an aqueous solution [21, 23–29].

2.2. Induced EF effect

According to Faraday's law, a time-variant MF will also induce a time-variant EF. The integral form of Faraday's law is as follows:

$$\oint_{l'} \vec{E} \cdot \mathrm{d}\vec{l'} = -\frac{\mathrm{d}}{\mathrm{d}t}\int_{S'''} \vec{B} \cdot \mathrm{d}\vec{S'''}, \tag{5}$$

where l' and S''' are the circumference of S''' and an arbitrary plane in the central region of the spiral inductor,

respectively. By considering the dimensions of specified cells, the magnitude of the induced EF resulting from the aforementioned time-variant MF can be calculated as follows:

$$\vec{E} = \frac{A}{C}\omega B_0 \sin\omega t \frac{\vec{x}_B}{|x_B|}, \tag{6}$$

where A and C are the contact area between cell and substrate and the circumference of cell, respectively. Similar to the approach for solving equation (1), the solution of oscillating displacement exerted by the induced EF will be [23]

$$x_E = \frac{zqA}{\lambda C} B_0 \sin\omega t. \tag{7}$$

The direction of x_E is normal to the surface of the plasma membrane.

Panagopoulos *et al* had proposed that significant electromagnetic force will act on the voltage sensor to interconvert the channel between closed and open states for ions to move within channel-proteins while the distance between the free ions and the voltage sensor of the voltage-gated channel is larger than 4×10^{-12} m [23]. Therefore, the superposition of x_B and x_E should satisfy the following condition to affect the cell signal transduction process:

$$x_B + x_E = \frac{\sqrt{3mkT}}{\lambda - zqB_0\cos\omega t} + \frac{zqA}{\lambda C} B_0 \sin\omega t \geqslant 4 \times 10^{-12}\text{m}. \tag{8}$$

Meanwhile, the net displacements normal to the surface of the plasma membrane in (8), the phases of ionic motion adopted in (2)–(4), and (7) should be carefully discussed as follows:

$$\begin{cases} x_E = 0 \\ x_B = 2\dfrac{\sqrt{3mkT}}{\lambda + zqB_0}, \qquad y_B = 2\dfrac{\sqrt{3mkT}}{\lambda - zqB_0} \\ z_B = 2\dfrac{\sqrt{3mkT}}{\lambda} \end{cases} \quad \text{for} \quad t = 0, \tag{9}$$

$$\begin{cases} x_E = 0 \\ x_B = \dfrac{\sqrt{3mkT}}{\lambda \pm zqB_0}, \qquad y_B = \dfrac{\sqrt{3mkT}}{\lambda \mp zqB_0} \\ z_B = \dfrac{\sqrt{3mkT}}{\lambda} \end{cases} \quad \text{for} \quad \omega t = n\pi,\ n = \begin{cases} \text{odd for } x_B : + \text{ and } y_B : - \\ \text{even for } x_B : - \text{ and } y_B : +, \end{cases} \tag{10}$$

$$\begin{cases} x_E = \dfrac{zqA}{\lambda C} B_0 \\ x_B = y_B = z_B = \dfrac{\sqrt{3mkT}}{\lambda} \end{cases} \quad \text{for} \quad \omega t = \frac{n}{2}\pi, \qquad n = \text{odd}. \tag{11}$$

The above equations reveal several significant results for bioactive effects under the ELF-EMF that are summarized as follows: (1) x_B, y_B and z_B have their maximum values when $t = 0$, so can explain why the EMF effects on the signal transduction process can be observed while the field is turned on or shut down [21], (2) the maxima of normal oscillating displacements, x_B and x_E, cannot exist simultaneously so that the bioactivity condition can only be contributed by either the time-variant MF or the induced EF, and (3) no matter what the phase is, the tangential oscillating displacement, y_B, related to the surface of the membrane always exists.

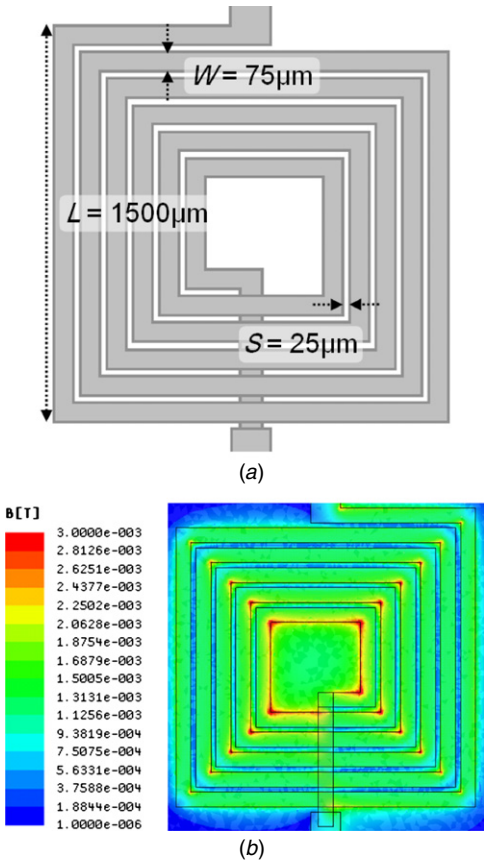

Figure 1. On-glass spiral inductor utilized for the ELF-EMF platform: (*a*) the scheme of the on-glass spiral inductor with the size of $L = 1.5$ mm, $S = 25$ μm and $W = 75$ μm, and (*b*) the distribution of the MF in the central region of the inductor.

3. Design and fabrication of the platform

3.1. Localized ELF-EMF platform design

For the investigation of the proximity effect on living cells resulting from the ELF-EMF exposure in this work, an on-chip spiral inductor as shown in figure 1 is designed, fabricated on a glass substrate and utilized for the generation of a localized time-variant MF concentrated at the central region of the inductor for cell culturing. Figure 1(*a*) shows a 5.5-turn coil inductor designed with $L = 1.5$ mm, $S = 25$ μm and $W = 75$ μm, respectively. Figure 1(*b*) shows the simulation result indicating that a 60 Hz and 1.2 mT MF is built in the central region of the inductor with a 60 Hz, 150 mA electrical input current. Ibrahim *et al* [22] have shown that the adopted input current source with a frequency of 60 Hz can generate an ELF-MF which has the same field strength as that generated

by a dc input. Thus, according to the concept of the quasi-electrostatic current source associated with the Biot–Savart law, an analytical model for characterizing the strength of the time-variant MF built by the spiral inductor in terms of the geometrical structure and amplitude of an input current is derived and verified by the Ansoft–Maxwell simulation and experimental measurement in this work. Using the integral forms of Maxwell's equations in the culturing medium where the inductor is located, the strength of the generated time-variant MF, $\vec{B}$, could be stated as follows:

$$\oint_l \frac{\vec{B}}{\mu_o} \cdot \mathrm{d}\vec{l} = \int_{S'} \vec{J}_{\mathrm{metal}} \cdot \mathrm{d}\vec{S'} + \int_{S''} \vec{J}_{\mathrm{bio}} \cdot \mathrm{d}\vec{S''} + \frac{\mathrm{d}}{\mathrm{d}t} \int_{S''} \varepsilon_{\mathrm{bio}} \varepsilon_o \vec{E} \cdot \mathrm{d}\vec{S''}, \tag{12}$$

where l, S' and S'' are the arbitrary closed loop (whose character length should be larger than the dimensions of the spiral inductor), the cross section of the inductor that current density in metal $\vec{J}_{\mathrm{metal}}$ can pass and the closed surface enclosed by the loop but excluding the cross section and current density in the biological material $\vec{J}_{\mathrm{bio}}$ that can pass, respectively. The parameters μ_o, $\varepsilon_{\mathrm{bio}}$, ε_o and $\vec{E}$ are the permeability for the entire system [23], the permittivity in the culturing medium, the permittivity in vacuum and EF, respectively.

In this case, because the inductor structure is coated with parylene-C, which is a good electrical insulator with the resistivity of 6×10^{16} Ω cm, to prevent electric current leakage into the cell culture medium and the wavelength of the introduced ELF-EMF is much larger than the dimensions of the spiral inductor, the second and third terms in (12) can be safely eliminated and the strength of the time-variant MF can, therefore, be further simplified as follows:

$$\oint_l \frac{\vec{B}}{\mu_o} \cdot \mathrm{d}\vec{l} = \int_S \vec{J}_{\mathrm{metal}} \cdot \mathrm{d}\vec{S}. \tag{13}$$

The simplified equation indicates that the behavior of the MF in the culturing medium would be similar to that in vacuum. For the calculation of the MF generated by the spiral inductor in the culturing platform, the inductor can be simply decomposed into several semi-symmetrical parts as shown in figure 2, so that the strength of the time-variant MF, B_1, at the central region of the inductor and the maximum field, B_2, at the inner corner can be simply expressed respectively as follows:

$$B_1 = B^{(\mathrm{I})} + B^{(\mathrm{II})} = \frac{1}{2} \sum_{n=1}^{2[m]+1} \frac{2\sqrt{2}\mu_0 I}{\pi} \frac{1}{L - nW - (n-1)S} \tag{14}$$

and

$$B_2 = B^{(\mathrm{III})} + B^{(\mathrm{IV})} + B^{(\mathrm{V})} + B^{(\mathrm{VI})} = \sum_{n=0}^{[m]} \frac{\mu_0 I}{4\pi} \left(\frac{2\sqrt{2}}{L_A^{(n)}} + \frac{2\sqrt{2}}{L_B^{(n)}} + 2\sqrt{\frac{1}{(L_A^{(n)})^2} + \frac{1}{(L_B^{(n)})^2}} \right), \tag{15}$$

where

$$L_A^{(n)} = L - ([m]+n)S - \left([m] + \tfrac{1}{2} + n\right)W, \tag{16}$$

$$L_B^{(n)} = ([m]-n)S + \left([m] + \tfrac{1}{2} - n\right)W. \tag{17}$$

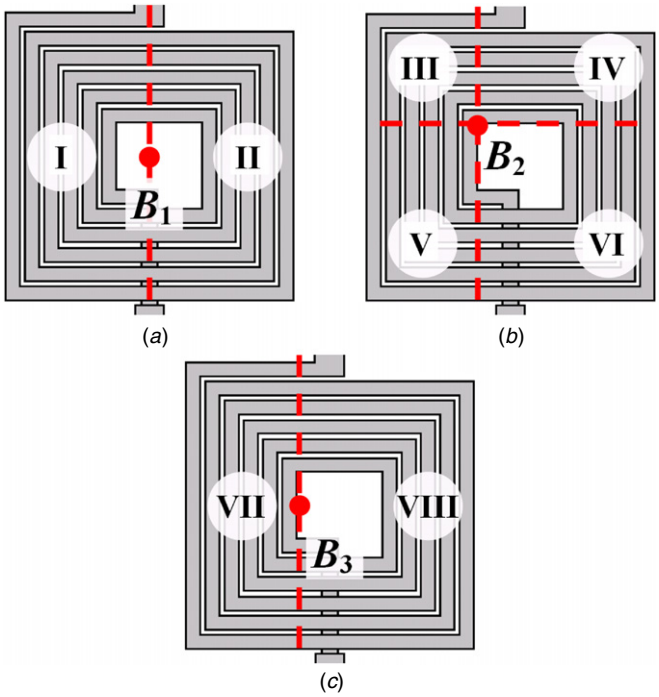

Figure 2. The decomposition of the spiral inductor for the estimation of MFs, B_1, B_2 and B_3 at (*a*) the central region, (*b*) the inner corner and (*c*) the inner middle of the inductor, respectively.

The parameters m, I, L, W and S are the circle number of the inductor, the input current, the length of the maximum edge, the width of metal and the metal spacing, respectively. The notation $[m]$ is a Gaussian symbol. The strength of the MF at the inner-middle edge in the central region, shown in figure 2(*c*), can have the following form:

$$\begin{aligned} B_3 &= B^{(\mathrm{VII})} + B^{(\mathrm{VIII})} \\ &= \sum_{n=0}^{[m]} \frac{\mu_o I}{2\pi} \left(\left[L_B^{(n)} \sqrt{1 + \left(\frac{L_B^{(n)}}{L_C^{(n)}} \right)^2} \right]^{-1} \right. \\ &\quad + 2 \left[L_C^{(n)} \sqrt{1 + \left(\frac{L_C^{(n)}}{2L_B^{(n)}} \right)^2} \right]^{-1} \\ &\quad + \left[L_A^{(n)} \sqrt{1 + \left(\frac{L_A^{(n)}}{L_D^{(n)}} \right)^2} \right]^{-1} \\ &\quad \left. + 2 \left[L_D^{(n)} \sqrt{1 + \left(\frac{L_D^{(n)}}{2L_A^{(n)}} \right)^2} \right]^{-1} \right), \end{aligned} \tag{18}$$

where

$$L_C^{(n)} = (L - W) - 2n(W + S), \tag{19}$$

$$L_D^{(n)} = L_C^{(n)} - (W + S). \tag{20}$$

For instance, by adopting the geometrical structure of the inductor shown in figure 1 with an input current of 150 mA,

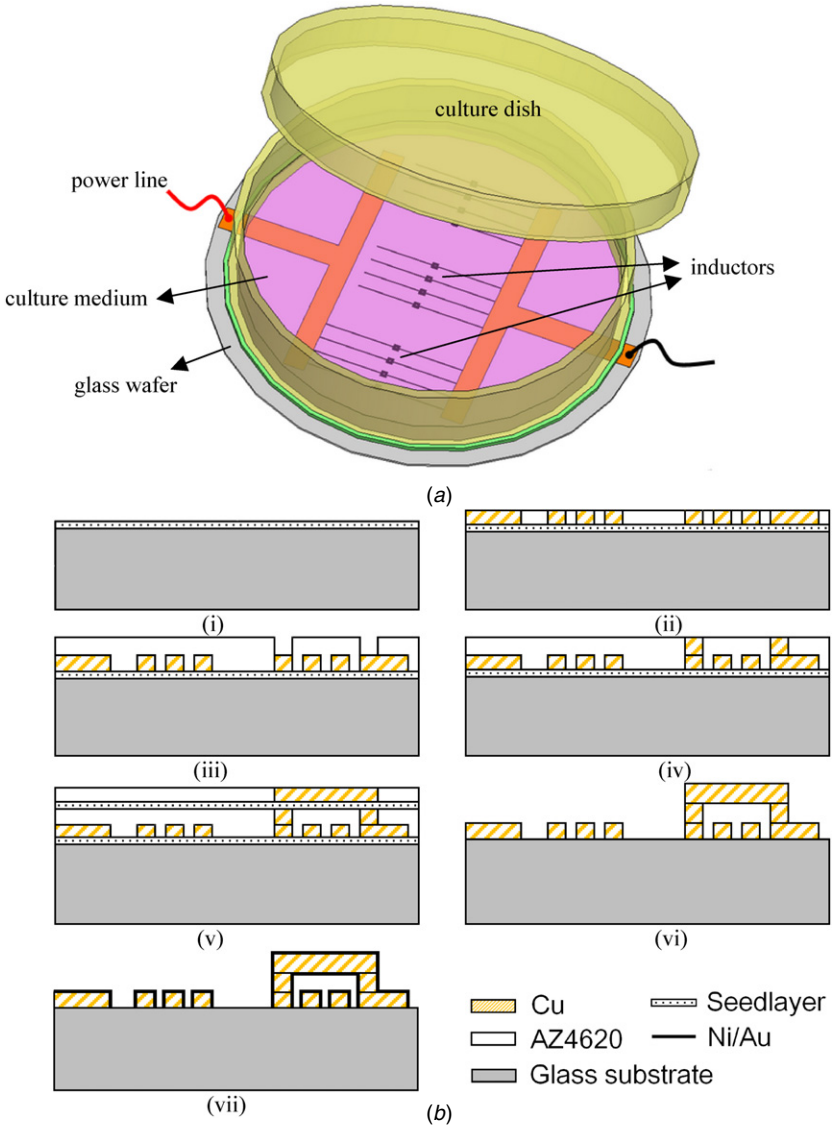

Figure 3. (*a*) Scheme of the proposed micro cell incubation system for investigation of the proximity effect of a time-variant MF on living cells. (*b*) Fabrication process of the spiral inductor.

the strength of the MFs derived in (14), (15), and (18) can be calculated as follows:

$$B_1 = B^{(\mathrm{I})} + B^{(\mathrm{II})} = 1.16\ (\mathrm{mT}),$$

$$B_2 = B^{(\mathrm{III})} + B^{(\mathrm{IV})} + B^{(\mathrm{V})} + B^{(\mathrm{VI})} = 3.70\ (\mathrm{mT}),$$

$$B_3 = B^{(\mathrm{VII})} + B^{(\mathrm{VIII})} = 2.20\ (\mathrm{mT}).$$

The above calculations reveal that a 5.5-turn spiral inductor driven by 150 mA input current can sustain at least 1 mT time-variant MF in the central region for following cell growth investigation.

Meanwhile, the presented platform design for the proximity effect study is constructed on a glass-based structure as shown in figure 3. An inductor array consisting of powered and unpowered subgroups in a culture dish is utilized to ensure that the cells are cultured in the same environment without suffering any salt concentration difference. To eliminate the possible electromagnetic interference within these inductors, the distance from center to center of the powered inductors is taken to be 2.5 mm, from which the MF can have two orders of magnitude reduction. Only less than 3% of the peak amplitude MF exists near the inner edge of the inductor based on the aforementioned calculation. In addition, the distance between the powered and unpowered subgroups is taken to be long, i.e. 13 mm, for better field isolation. It is noted that a glass wafer is glued with a hollow culture dish to form a micro cell incubator where the inductors are fabricated on the substrate and coated with a biocompatible layer, i.e. parylene-C, for cell attachment. The platform design can effectively facilitate the observation of cell growth from the backside of the substrate without having any contamination issues, since the incubator can be covered by a polystyrene lid during cell growth to prevent undesired particles and bacteria from falling into the culture medium.

Figure 3(*b*) depicts the fabrication processes of the platform. A Cr/Cu (300 Å/900 Å) layer is first sputtered onto a 4″ glass wafer as an adhesion/seed layer as shown in

figure 3(*b*-i). A layer of 10 μm thick AZ4620 photoresist is then spin-coated and photolithographically patterned on the adhesion/seed layer as a mold for inductor coil fabrication using Cu electroplating as shown in figure 3(*b*-ii). Figure 3(*b*-iii) shows that another 10 μm thick AZ4620 photoresist is then spin-coated and patterned on the coil structure to define a via hole filled by electroplated Cu. Once the via is filled by electroplating as shown in figure 3(*b*-iv), another copper seed layer (1500 Å) for air bridge fabrication is deposited, and then coated with a 12 μm thick AZ4620 photoresist followed by 10 μm Cu plating as shown in figure 3(*b*-v). After the inductor is fabricated, the photoresist and seed layers are removed by acetone and Cr-7T. In order to prevent Cu corrosion occurring in the culture medium, an immersion process [24] is utilized to coat a layer of Ni (0.25 μm)/Au (50 nm) on the top of the Cu structure as shown in figure 3(*b*-vi). Parylene-C is a biocompatible, transparent, nontoxic and chemically inert material. Previous study has shown that parylene-C is a highly conformal layer of stable microelectrode insulator [25]. Therefore, it is chosen for the electrical insulation coating in this work. The as-fabricated device substrate is first put into adherent agent (A-174) for 15 min and then into the polymer deposition system (Speedline Tech, PDS 2010) for 0.5 μm parylene-C deposition.

A gaussmeter (TM601, Kanetec, Japan) is utilized for the validation of our design regarding the characteristics of the time-variant MF. Figure 4 shows the comparison between measurement and simulation results of the MF strength in the central region of the inductor with the aforementioned 5.5-turn design. The excellent agreement shown in figure 4(*a*) indicates that the measured MF strength indeed follows the prediction of the theoretical calculation based on equation (14). Meanwhile, the theoretical calculation is verified using a Maxwell 3D field simulator (Ansoft LLC, Pittsburgh, PA, USA) as shown in figure 4(*b*). Precise prediction in terms of profile and magnitude has revealed the practicality of the presented model. Furthermore, a group of inductors with the same geometry are designed and fabricated on the microplatform to simultaneously control the culturing conditions and environment for comparative investigation. According to the spatial gradient of the MF as shown in figure 4(*a*), the strength of the MF would decay to 30% of the field strength at the central region, while the observed point is away from the region with a critical distance of at least 500 μm. Thus, the adopted spacing of each inductor in the design is 2.5 mm which is five times the 500 μm distance and can effectively isolate every operating inductor without having any field interference. Each inductor can safely be treated as a purely single micro-incubator for cell culturing with the same MF, i.e. ∼1.2 mT in this work.

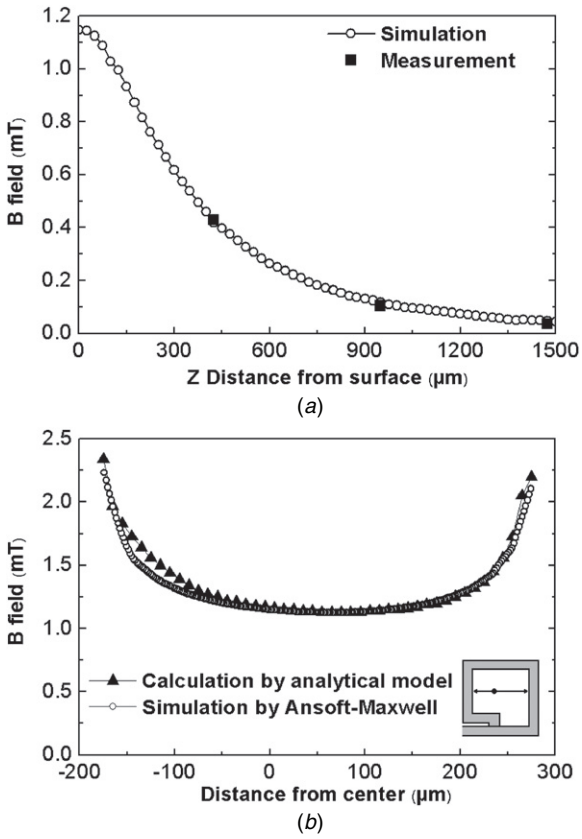

Figure 4. (*a*) Measured MF strength perfectly matched with the decay trend from the Biot–Savart law. (*b*) The distribution of the localized MF calculated by the analytical model and simulated by Ansoft-Maxwell.

3.2. Thermal analysis

According to equations (14), (15) and (18), the input electric current is a critical parameter for generating the localized ELF-MF. Owing to the finite resistivity of the Cu inductor, the input current will also cause the inevitable thermal effect due to associated Joule heating at the junction between the inductor and its outside environment while the MF is generated. According to the finite element method simulation as shown in figure 5, most of the heat generated by the coils can directly pass through the glass substrate, and then dissipate into the stainless steel plate below the substrate. Thus, for better thermal conduction, the thickness of the glass substrate is chosen to be 500 μm in the platform fabrication which can not only provide the shortest thermal flow path from the spiral inductor to itself but also maintain the rigidity of the whole incubation system. In addition, the culturing medium could also play the role of preserving the bulk temperature by thermal convection due to its large specific heat capacitance.

An Ansoft-ePhysics simulator (Ansoft LLC) is employed for the thermal analysis to predict the maximum cell culturing temperature based on the platform design. In this work, the platform is kept in an incubator under the conditions of 36 °C, 5% CO_2 atmosphere and 100% humidity for the cell proliferation investigation. Figure 5(*a*) shows the simulated surface temperature of the 5.5-turn spiral inductor immersed in deionized water with different input currents. For a current input of 150 mA, there is an ∼0.9 °C temperature rise within the inductor that compares well with the experimental results measured by a Digi-Sense thermometer. Nevertheless, the temperature difference between the simulation and measurement can be attributed to the size of the sensing probe which covers the entire inductor and makes the measured temperature lower than that of the simulation.

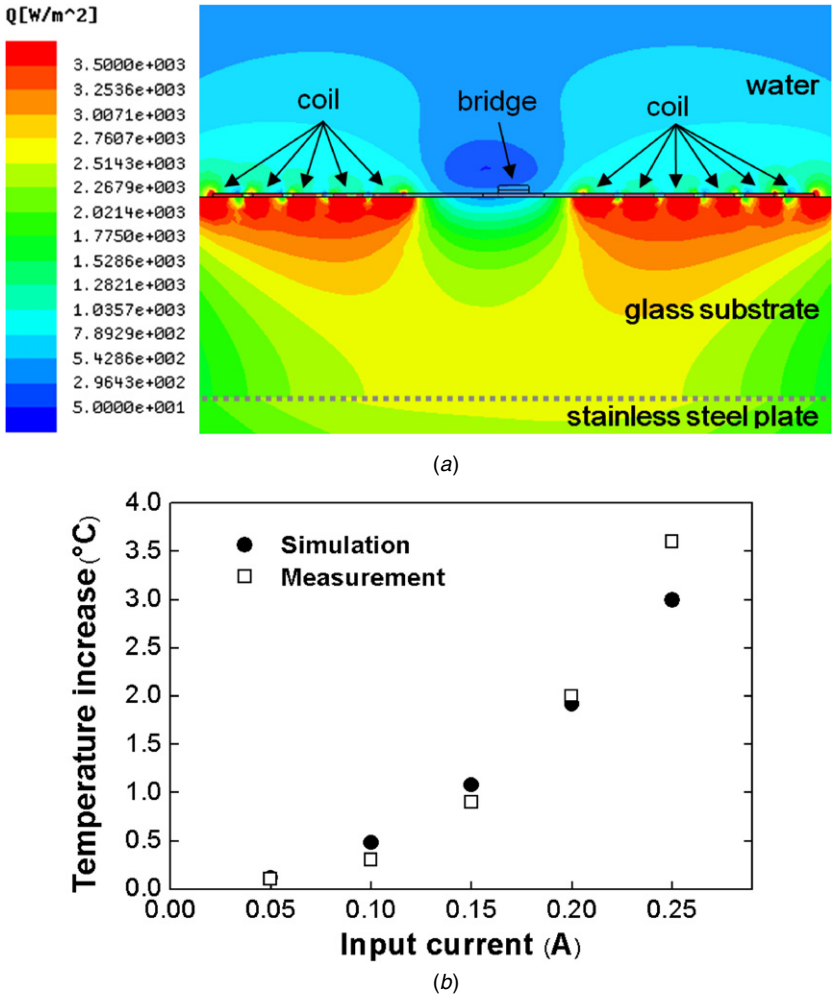

Figure 5. Thermal analysis of the platform. (*a*) Thermal flux simulation indicating that the major heat flow is conducted to the bottom stainless steel plate via the glass substrate. The stainless steel plate can effectively maintain surface temperature. (*b*) Temperature increase measured by a thermometer and simulated by Ansoft-ePhysics at different input currents.

3.3. Preparation of cell culture

The parylene-C surface is treated with oxygen plasma for 30 s for surface property modification from hydrophobic to hydrophilic. The plasma treatment can keep the surface hydrophilic for a long time [26], which can benefit protein adsorption for cell adhesion and spreading for long-term cell proliferation and observation. Finally, 15 min UV exposure is performed to sterilize the whole culture system, which is followed by the immersion in 10% poly-D-lysine protein in phosphate-buffered saline (PBS) liquid solution for cell culturing.

HeLa and PC-12 cells (CRL-1721 TM) are supplied by National Health Research Institutes (NHRI). The HeLa cells are cultured in Dulbecco's modification of the Eagle medium (Gibco, DMEM 119955-065) with 10% fetal bovine serum (FBS), and the PC-12 cells are cultured in the RMPI-1640 medium (HyClone, SH30027). The volume of additive culture media is 20 mm^3. After the pre-treatment for placement of cells on the surface of the microplatform, the platform is put in an incubator with humidified atmosphere of 5%/95% CO_2/air (Sanyo, MCO-20AIC) at 37 °C. After waiting 10 h for cell adhesion, the platform is connected to an ac current source (Alger, CW301), which will provide a 150 mA, 60 Hz electric current input to the inductor. Meanwhile, the bulk temperature of the incubator is modified from 37 to 36 °C to kept the hot spot lower than 37 °C. It also means that the control group of the inductor without the localized ELF-EMF is kept at 36 °C.

4. Results and discussion

A localized ELF-EMF is applied continuously on living cells that adhere and grow at the central area of the inductor for 72 h. The cell culturing status is observed by an inverted optical microscope every 24 h. Cell proliferation based on three experimental groups with field exposure and two control groups without field exposure is calculated using the cell counter function of the ImageJ software (National Institutes of Health, http://rsb.info.nih.gov/ij/;). Figure 6 shows optical micrographs of HeLa cell growth from $t = 0$ to 72 h. It is observed that the total cell amount at a localized magnetic area is not the same as that at the initial states and fewer cells proliferate under MF exposure. For fair comparison,

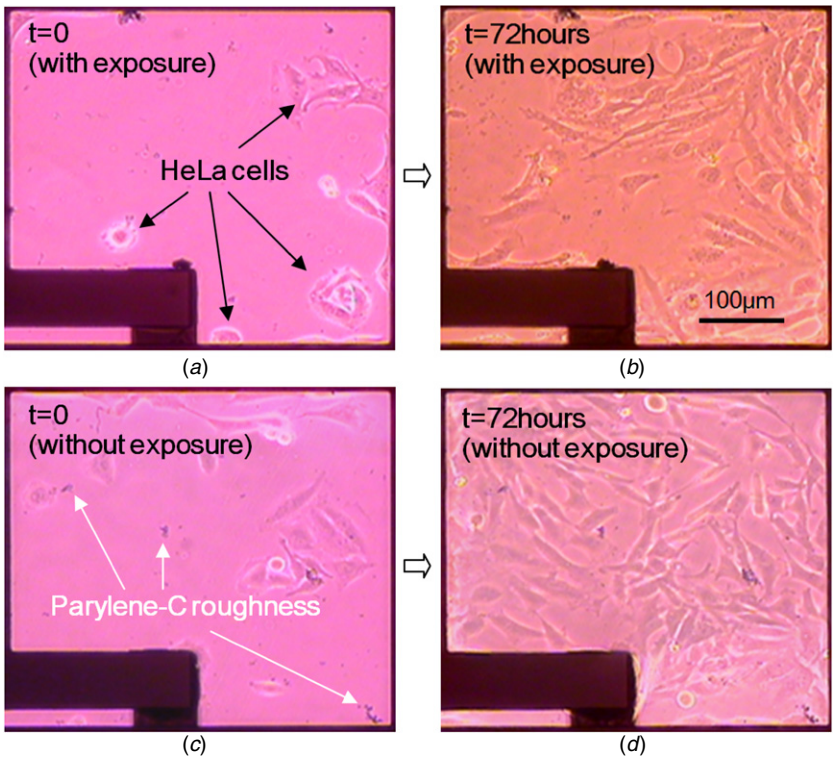

Figure 6. Optical micrographs of HeLa cell growth. Exposed group at (*a*) $t = 0$ and (*b*) $t = 72$ h. The group without exposure at (*c*) $t = 0$ and (*d*) $t = 72$ h.

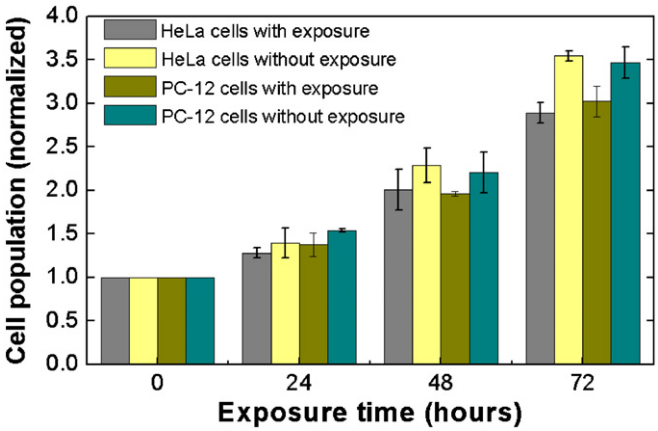

Figure 7. Cell density (normalized to the initial density of each inductor) of the exposed group compared to the control group without the ∼1.2 mT, 60 Hz localized MF.

the difference of total cell amount at the central area of each spiral inductor with/without time-variant MF exposure is normalized by the initial amount of cells. The cell density is estimated as

$$\text{Cell density}_{\text{normalized}} = \frac{\text{Amounts}_{\text{time}=N\text{ hrs}}}{\text{Amounts}_{\text{time}=0\text{ hrs}}}. \tag{21}$$

Figure 7 shows the results of cell proliferation of HeLa and PC-12 cells both from the experimental and control groups, and the error bars are based on the 95% confidence interval calculated by the average number, standard error and sample counts of these groups. The variations of cell density shown as follows are defined and utilized for the comparison of cell proliferation between the average amounts in the exposed and control groups:

$$\text{Variation of cell density}(\%) = \left[\frac{(\text{Amounts}_{t=N\text{hrs}} - \text{Amounts}_{t=0\text{ hrs}})_{\text{exposure}}}{(\text{Amounts}_{t=N\text{ hrs}} - \text{Amounts}_{t=0\text{hrs}})_{\text{control}}} - 1\right] \times 100\%. \tag{22}$$

Table 1 lists the comparison between the exposed and control groups in terms of exposure time and variation of cell density. The results indicate that the localized MFs will affect the cell proliferation, which decreases with the increase of exposure time in a nonlinear relationship. There is no significant difference in the cell proliferation of the HeLa cells after 24 and 48 h field exposure. However, a proliferation decrease occurring after 72 h field exposure reveals that the HeLa cell proliferation would be affected by a long-term

Table 1. Difference in the proliferation rate of HeLa and PC-12 cells in comparison with the groups with and without ELF-EMF exposure for different time periods.

	Change in the cell proliferation rate (%)	
Exposed time (h)	HeLa cells	PC-12 cells
0	0	0
24	−8.3	−10.7
48	−12.1	−11.0
72	−18.4	−12.9
	$P = 0.056$	$P = 0.077$

exposure to the ELF-EMF. On the other hand, the experimental results of the PC-12 cells show that an obvious proliferation decrease takes place at the beginning and would continue decreasing for 72 h. Additionally, 37 °C is the most suitable growth temperature for cells. A higher or lower temperature environment will generally suppress the cell growth rate. About 1 °C temperature difference is a crucial factor for the cell mitotic cycle. In 1996, Chuppa *et al* reported that the culturing temperature decrease would result in a 4.1% specific growth rate decrease in hamster cells when the temperature was lowered down to 35.5 °C from 37 °C [30]. In 2004, Mazza *et al* provided a thermal dose determination which had shown that human fetal lung cells cultured at 36 °C would have a 7.8% doubling rate decrease in comparison with that at 37 °C [31]. In fact, HeLa cells also showed the same tendency in temperature-controlled experiments. In 1965, Rao *et al* reported the temperature effect on the life cycle of HeLa cells [32]. The generation time of the culture temperature, 36 °C, is 25.8 h in contrast to 21.8 h for 37 °C. The growth rate at 36 °C is about 18% lower than that at 37 °C. In the experimental setup, the best growth temperature is set for the exposed group, which is controlled at 37 °C. According to the observation, the exposed group has a lower growth rate in comparison with the control group whose growth temperature is about 36 °C. Since 37 °C is the most suitable culturing temperature for a living cell and cell mitotic rate decreases at a temperature lower than this value, therefore, the observation evidences the ELF-EMF influence that strongly suppresses the cell proliferation. Although one way ANOVA (F-test) in SPSS version 17.0 (SPSS Inc., Chicago, IL) has shown that the P-value in our experiment as listed in table 1 is larger than 0.05, indicating no obviously significant cell growth rate difference owing to small sample numbers, the experimental results still present the possible tendency of cell growth under a localized ELF-EMF.

By combining (8), (9), (11) and (14), the net normal displacement is about 7.2×10^{-12} m dominated by the x_B while the applied time-variant MF is 1.2 mT, 60 Hz for our case. As aforementioned, the value larger than 4×10^{-12} m indicates that the field will disturb the bioactivity of cells by affecting cell signal transduction process. The disturbance of the signal transduction process resulting from the time-varying MF of the ELF-EMF could be one of the possible mechanisms inhibiting cell growth. In addition, similar to the concept of electrostatic screening occurring in crystals, the inhibited growth phenomenon of the cells resulting from a bioactivity process interference can be partly attributed to the tangentially ionic motion governed by the ELF-EMF. All oscillating ions in the vicinity of the extracellular membrane with a net tangential displacement, y_B, could be treated as ring-like currents enclosing the cells and partially screening ionic flux into or out of the cellular membrane, so that the signal transduction process will also be interfered with and eventually fail. Nevertheless, ELF-EMF field exposure time, field strength and the types of cells are various factors leading to different results. Further investigation regarding the proximity effect of the ELF-EMF on cell growth is still required and can be continued using the proposed microplatform.

5. Conclusions

A bio-compatible microplatform has been designed and utilized for the proximity effect investigation of ELF-EMF effects on cell growth. An analytical model for the prediction of a localized ELF-EMF on the microplatform is provided for rapid application, modification and optimization. Experimental results show 18.4% and 12.9% proliferation decrease of HeLa cells and PC-12 cells after 72 h exposure to an ∼1.2 mT, 60 Hz ELF-EMF, respectively. The proliferation rate reduction can be attributed to the interference of the signal transduction process. According to the theoretical calculation of ionic motion in living cells affected separately by the time-variant MF and induced EF of the associated ELF-EMF, it has been theoretically found that the oscillating motion of ions normal to the surface of a cell's plasma membrane could exert a significant electromagnetic force acting on the voltage sensors in the voltage-gated channels, and the motion tangential to the membrane would effectively screen ionic flux into or out of the cellular membrane. Both effects will possibly result in interference with and failure of the signal transduction process of cells to inhibiting cell proliferation.

Acknowledgments

The authors would like to thank NHRI for providing cells and Nano/Micro Bio-Opto-Electro-Mechanical Systems and Fluidics Laboratory for supplying instruments for experiments. They would also like to thank NCHC and NCTU for thermal and magnetic analysis software.

References

[1] Feychting M, Forssen U, Rutqvist L E and Ahlbom A 1998 Magnetic fields and breast cancer in Swedish adults residing near high-voltage power lines *Epidemiology* **9** 392–7

[2] Draper G, Vincent T, Kroll M E and Swanson J 2005 Childhood cancer in relation to distance from high voltage power lines in England and Wales: a case-control study *Br. Med. J.* **330** 1290–4

[3] Katsir G, Baram S C and Parola A H 1998 Effect of sinusoidally varying magnetic fields on cell proliferation and adenosine deaminase specific activity *Bioelectromagnetics* **19** 46–52

[4] Heredia-Rojas J A, Rodríguez-De la Fuente A O, del Roble Velazco-Campos M, Leal-Garza C H, Rodríguez-Flores L E and de la Fuente-Cortez B 2001 Cytological effects of 60 Hz magnetic fields on human lymphocytes *in vitro*: sister-chromatid exchanges, cell kinetics and mitotic rate *Bioelectromagnetics* **22** 145–9

[5] Khalil A M and Qassem W 1991 Cytogenetic effects of pulsing electromagnetic field on human lymphocytes *in vitro*: chromosome aberrations, sister-chromatid exchanges and cell kinetics *Mutat. Res.* **247** 141–6

[6] Kwee S and Raskmark P 1995 Changes in cell proliferation due to environmental non-ionizing radiation: 1. ELF electromagnetic fields *Bioelectrochem. Bioenerg.* **36** 109–14

[7] Wolf F I, Torsello A, Tedesco B, Fasanella S, Boninsegna A, D'Ascenzo M, Grassi C, Azzena G B and Cittadini A 2005 50-Hz extremely low frequency electromagnetic fields enhance cell proliferation and DNA damage: possible involvement of a redox mechanism *Biochim. Biophys. Acta* **1743** 120–9

[8] Buemi M *et al* 2001 Cell proliferation/cell death balance in renal cell cultures after exposure to a static magnetic field *Nephron* **87** 269–73
[9] Huang L, Dong L, Chen Y, Qi H and Xiao D 2006 Effects of sinusoidal magnetic field observed on cell proliferation, ion concentration, and osmolarity in two human cancer cell lines *Electromagn. Biol. Med.* **25** 113–26
[10] Bayrashev A, Robbins W P and Ziaie B 2004 Low frequency wireless powering of microsystems using piezoelectric–magnetostrictive laminate composites *Sensors Actuators* A **114** 244–9
[11] Kurs A, Karalis A, Moffatt R, Joannopoulos J D, Fisher P and Soljacic M 2007 Wireless power transfer via strongly coupled magnetic resonances *Science* **317** 83–6
[12] Harrison R R, Watkins P T, Kier R J, Lovejoy R O, Black D J, Greger B and Solzbacher F 2007 A low-power integrated circuit for a wireless 100-electrode neural recording system *IEEE J. Solid-State Circuits* **42** 123–33
[13] Kricka L J 2001 Microchips, microarrays, biochips and nanochips: personal laboratories for the 21st century *Clin. Chim. Acta* **307** 219–23
[14] Medoro G, Manaresi N, Leonardi A, Altomare L, Tartagni M and Guerrieri R 2003 A lab-on-a-chip for cell detection and manipulation *IEEE Sens. J.* **3** 317–25
[15] Hung P J, Lee P J, Sabounchi P, Aghdam N, Lin R and Lee L P 2005 A novel high aspect ratio microfluidic design to provide a stable and uniform microenvironment for cell growth in a high throughput mammalian cell culture array *Lab Chip* **5** 44–8
[16] Tourovskaia A, Figueroa-Masot X and Folch A 2005 Differentiation-on-a-chip: a microfluidic platform for long-term cell culture studies *Lab Chip* **5** 14–9
[17] Walker G M, Ozers M S and Beebe D J 2002 Insect cell culture in microfluidic channels *Biomed. Microdevices* **4** 161–6
[18] Tsurita G, Ueno S, Tsuno N H, Nagawa H and Muto T 1999 Effects of exposure to repetitive pulsed magnetic stimulation on cell proliferation and expression of heat shock protein 70 in normal and malignant cells *Biochem. Biophys. Res. Commun.* **261** 689–94
[19] Blackman C F, Blanchard J P, Benane S G and House D E 1994 Empirical test of an ion parametric resonance model for magnetic field interactions with PC-12 cells *Bioelectromagnetics* **15** 239–60
[20] Ando J, Smith N I, Fujita K and Kawata S 2009 Photogeneration of membrane potential hyperpolarization and depolarization in non-excitable cells *Eur. Biophys. J.* **38** 255–62
[21] Jia M, Minxu L, Liu X W, Jiang H, Nelson P G and Guroff G 1999 Voltage-sensitive calcium currents are acutely increased by nerve growth factor in PC12 cells *J. Neurophysiol.* **82** 2847–52
[22] Ibrahim N M and Kuhn W B 2002 An approach for the calculation of magnetic field within square spiral inductors at low frequency *Int. J. Numer. Modelling* **15** 339–54
[23] Panagopoulos D J, Karabarbounis A and Margaritis L H 2002 Mechanism for action of electromagnetic fields on cells *Biochem. Biophys. Res. Commun.* **298** 95–102
[24] Rohan J F, O'Riordan G and Boardman J 2002 Selective electroless nickel deposition on copper as a final barrier/bonding layer material for microelectronics applications *Appl. Surf. Sci.* **185** 289–97
[25] Loeb G E, Bak M J, Salcman M and Schmidt E M 1977 Parylene as a chronically stable, reproducible microelectrode insulator *IEEE Trans. Biomed. Eng.* **24** 121–8
[26] Chang T Y, Yadav V G, De Leo S, Mohedas A, Rajalingam B, Chen C L, Selvarasah S, Dokmeci M R and Khademhosseini A 2007 Cell and protein compatibility of parylene-C surfaces *Langmuir* **23** 11718–25
[27] Ando J, Smith N I, Fujita K and Kawata S 2009 Photogeneration of membrane potential hyperpolarization and depolarization in non-excitable cells *Eur. Biophys. J.* **38** 255–62
[28] Baker P F, Hodgkin A L and Shaw T I 1962 The effects of changes in internal ionic concentrations on the electrical properties of perfused giant axons *J. Physiol.* **164** 355–74
[29] Chiabrera A, Bianco B, Moggia E and Tommasi T 1994 Interaction mechanism between electromagnetic fields and ion adsorption: endogenous forces and collision frequency *Bioelectrochem. Bioenerg.* **35** 33–7
[30] Chuppa S, Tsai Y S, Yoon S, Shackleford S, Rozales C, Bhat R, Tsay G, Matanguihan C, Konstantinov K and Naveh D 1996 Fermentor temperature as a tool for control of high-density perfusion cultures of mammalian cells *Biotechnol. Bioeng.* **55** 328–38
[31] Mazza S, Battaglia L F, Miller M W, Dewey W C, Edwards M J and Abramowicz J S 2004 The ΔT thermal dose concept 2: *in vitro* cellular effects *J. Therm. Biol.* **29** 151–6
[32] Rao P N and Engelberg J 1965 HeLa cells: effects of temperature on the life cycle *Science* **148** 1092–4